To cite this article: Wang K, Duan Y T, Shi L H, et al. Design and realization of a nearby lightning-electric field environment simulator[J]. Chinese Journal of Ship Research, 2019, 14(5). http://www.ship-research.com/EN/Y2019/V14/I5/119.

DOI: 10.19693/j.issn.1673-3185.01368

Design and realization of a nearby lightning-electric field environment simulator

Wang Ke, *Duan Yantao**, *Shi Lihua*, *Huang Ruitao*, *Chen Hailin*

National Key Laboratory on Electromagnetic Environment Effects and Electro-Optical Engineering, Army Engineering University of PLA, Nanjing 210007, China

Abstract: [**Objectives**] Lightning can be extremely harmful to ships on the open seas. Especially with the large-scale application of electronic and electrical equipment and closed integrated masts, the lightning indirect effect on ships is becoming increasingly serious. In order to effectively carry out the lightning indirect effect test for shipborne electrical and electronic equipment, [**Methods**] a kind of nearby lightning-electric field environment simulator based on the principle of Marx generator was designed and realized in this paper. The simulator realized the peak cut-off of the impact high voltage by using the adjustable single chopping sphere gap, and established a simulated nearby lightning-electric field environment through the high voltage plate and the conductive ground plane. [**Results**] The test results show that the device has a cut-off time of less than 2 μs and a drop time of less than 0.09 μs, which can produce a pulsed electric field environment that meets the requirements of GJB 1389A-2005. [**Conclusions**] This paper can provide equipment support for the research on the indirect effect of the nearby lightning strokes on system electronic and electrical equipment based on GJB 8848-2016.

Key words: Marx generator; nearby lightning strike; pulsed electric field; lightning indirect effects

CLC number: U674.7+02; N33

0 Introduction

Lightning is a common natural discharge phenomenon, often accompanied by complex changing electromagnetic environments. In the open seas with complicated and changeable climate, the operation of tall masts and various types of protruding antennas on ships are very likely to attract lightning during thunderstorms, which will cause great damage to shipboard electronic and electrical equipment [1-3]. Thomson [4] analyzed 71 incidents of lightning strikes on ships in open seas and pointed out that the characteristics of the ships themselves and the special environment in which they are located are the important reasons for the lightning strikes. In recent years, the media has often reported accidents with significant losses in the southeast coastal areas of China that shipborne radar and other equipment encountered

Received: 2018-12-13

Supported by: National Key Research and Development Project (2017YFC1501505)

Authors: Wang Ke, male, born in 1995, master. Research interest: electromagnetic protection theory and technology. E-mail: 1363611280@qq.com

Duan Yantao, male, born in 1980, Ph.D.. Research interest: electromagnetic protection and electromagnetic simulation. E-mail: dcmchdyt@126.com

Shi Lihua, male, born in 1969, Ph.D., Professor. Research interest: electromagnetic protection and electromagnetic compatibility. E-mail: lihuashi@aliyun.com

Huang Ruitao, male, born in 1994, master. Research interest: electromagnetic effect and protection of lightning. E-mail: 190485346@qq.com

Chen Hailin, male, born in 1979, Ph.D., associate professor. Research interest: electromagnetic protection and electromagnetic simulation. E-mail: ylinchen@126.com

***Corresponding author:** Duan Yantao

lightning strikes [5]. Therefore, lightning protection has great research value and practical significance for shipboard electronic and electrical equipment.

Lightning damage to ships mainly includes the direct and indirect effects. Lightning direct effects mainly refer to the physical effects caused by the direct attachment of lightning channels or the conduction of lightning current, which are manifested as combustion, explosion, erosion, high-voltage shock waves, structural deformation, and magnetic fields formed by strong currents. The lightning indirect effects are derived from the interaction between the electromagnetic field generated by lightning and shipborne equipment, including indirect effects caused by direct lightning strikes and nearby lightning strikes [6].

With the widespread use of various microelectronic and electrical equipment and complex electronic and electrical systems such as large-scale integrated circuits in equipment, shipboard equipment has more stringent requirements for the electromagnetic environment. The electromagnetic environment generated by a nearby lightning strike poses a real threat to these electronic and electrical systems. GJB 1389A-2005 Electromagnetic compatibility requirements for systems of China clearly points out the environmental parameters of the lightning indirect effects. The system should be able to withstand the lightning indirect effect in the exposed state, and it should pass the tests and verification of the system, sub-system, equipment, and component levels [7]. Aiming at the lightning environment requirements in GJB 1389A-2005, GJB 8848-2016 Electromagnetic Environmental Effects Test Methods for Systems clarifies the lightning test methods, test configurations, test procedures, and the evaluation criteria for test results. This provides a reference for the systematic lightning test, including the test method of electric field environment effect caused by nearby lightning strikes [8]. The NPFC MIL-STD-464C and NATO AECTP-500 [9-10] also have the same expression in their content on lightning protection requirements. At the same time, the US L3 Technologies has developed a near-field lightning simulator for the military to simulate the near-field electromagnetic field of the lightning channel and established the electric and magnetic fields caused by nearby lightning strikes for full-scale field testing of aircraft, missiles, and other equipment. In China, the research on the environmental effects of nearby lightning-pulse electromagnetic fields starts late. At present, there is no report on the development of related simulation equipment.

This paper intends to establish an electric field environment simulator for nearby lightning strikes through the peak cut-off of impulse high-voltage so as to provide technical support for full-scale field tests of system electronic and electrical equipment.

1 Basic principle

The simulation device for the pulsed electric field is mainly composed of an impulse high-voltage source, a cut-off device, a test platform, and a measurement control system. The equipment construction is shown in Fig. 1. Among them, the impulse high-voltage source is used to generate impulse high-voltage, and the cut-off device is used to cut off the impulse high-voltage to form a steep wave in the discharge circuit. The test platform is used to carry the test object and generate a uniform pulsed electric field environment that meets the requirements. The measurement control system is mainly used for monitoring working status and collecting test data.

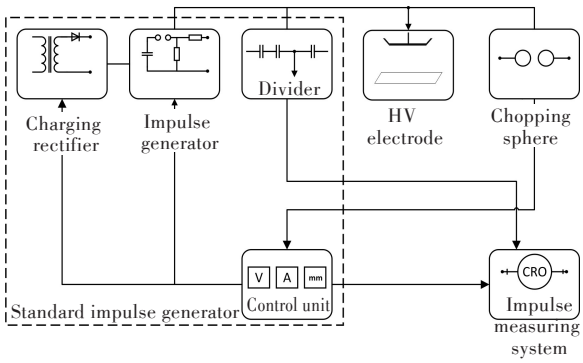

Fig.1 Schematic diagram of electric field environment simulator for nearby lightning strike

The working principle of the simulation device for the pulsed electric field can be briefly described as follows. First, the impulse high-voltage source is charged to form an impulse high-voltage of a certain amplitude on the high-voltage electrode. Destructive discharge occurs when the voltage at both ends of the chopping sphere is higher than the breakdown voltage of the air gap, and the impulse high-voltage rapidly decays to form a steep wave in the drop section. Thus, the voltage on the high-voltage electrode drops rapidly, thereby forming a rapidly changing electric field on the test platform. Through parameter design, this fast-changing electric field can reach the required value of GJB 1389A-2005 on the time change rate of the electric field, i.e., 6.8×10^{11} V/(m·s^{-1}).

2 Design of simulator for pulsed electric field

2.1 Impulse high-voltage source

Due to the limitation of the rated voltage of the high-voltage silicon stack and the energy-storage capacitor, the single-stage impulse voltage generator is difficult to meet the amplitude of the pulsed electric field. In this paper, a high-efficiency 8-stage Marx generator with bilateral charging is used as the impulse high-voltage source (Fig. 2) [11]. In the figure, K is a power switch; D is a high-voltage silicon stack, T_1 is a single-phase voltage regulator; T_2 is a test transformer; R_0 is a protection resistor; R is a charging resistor; r_f is a wave front resistor; r_t is a wave tail resistor; C is the charging capacitor at each level; C_2 is the test object capacitor; g_1 is the ignition sphere gap; g_2–g_8 are the intermediate sphere gaps; g_0 is the isolation sphere gap; C_{11} and C_{12} are the high-voltage arm capacitors of the capacitive voltage divider; C_{20} is the low-voltage arm capacitor of capacitive voltage divider.

The basic principle is as follows: the charging capacitor C is discharged in series after being charged in parallel on both sides. After the isolation sphere gap g_0 is broken through, an impulse voltage wave with multiple amplitudes is obtained on the discharge circuit. Bilateral parallel charging is achieved through two reverse-connected silicon rectifier stacks, while series discharge is achieved through a set of well-synchronized sphere gap breakdowns.

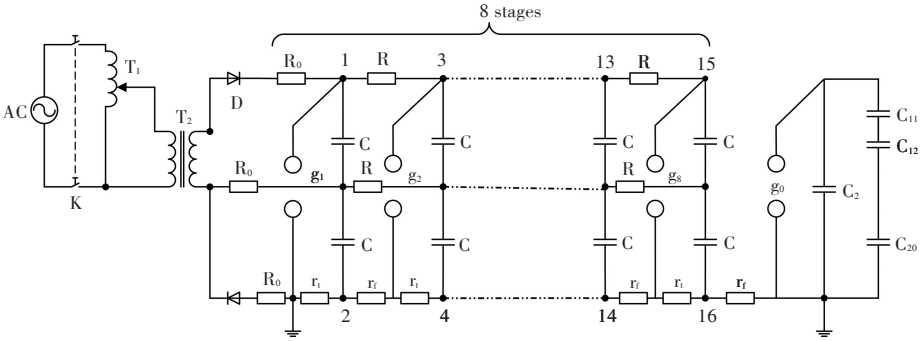

Fig.2 Bilaterally charged high efficiency Marx generator circuit

At present, the current Marx generator in the laboratory has a rated voltage of 75 kV for each charging capacitor with a total of 8 stages and can output a positive and negative impulse voltage of 1 200 kV. At the same time, by adjusting the wave front resistance and wave tail resistance, the Marx generator can obtain the standard 1.2/50 μs lightning full-wave [12].

2.2 Cut-off device

Using the self-discharge of the sphere gap, the cut-off device plays a role of cut-off near the peak of impulse high-voltage in the discharge circuit, as shown in Fig. 3. For the pulsed electric field simulator, its cut-off characteristics must meet the following requirements: 1) The waveform does not produce front-end distortion under the influence of the pre-discharge process of the gap. 2) The cut-off time is as close to the waveform peak as possible and has repeatable, namely ensuring the cut-off near the peak and the minimum dispersity. 3) The drop time of voltage is as short as possible, and the steepness of the voltage drop is greater than 6.8×10^2 kV/μs to meet the design requirements.

Fig.3 Chopping sphere

Based on the above requirements, the cut-off device adopts a set of adjustable single chopping sphere gaps. The single chopping sphere gap makes the drop time as short as possible, and the adjustable chopping sphere gap makes the time change rate of the electric field continuously adjustable. The sphere gap can be matched according to the size of the charging voltage and adapted to the ignition sphere gap of Marx generator, so as to finally ensure that the cut-off characteristic of impulse high-voltage meets the requirements [11]. However, the free-triggered cut-off device is random to the

cut-off of the discharge waveform. Its dispersity is mainly related to the sphere gap, and the voltage drop time is mainly related to the voltage action time, the impulse polarity and the gap structure. Both are affected by the temperature, humidity, and gas density of the test environment [13]. Therefore, their parameter design should be considered from multiple aspects, and the actual measurement results shall prevail. According to the measured results, when the impulse voltage of positive polarity is 120-320 kV, the designed cut-off device has a cut-off time within 2 μs for all 1.2/50 μs lightning full waves, and the drop time of cut-off voltage is shorter than 0.09 μs, with good repeatability.

2.3 Test platform

The test platform consists of a high-voltage electrode and a conductive ground plane. The test space between them can generate a uniform electric field environment and carry the test object, as shown in Fig. 4. When the voltage on the high-voltage electrode drops rapidly, a rapidly changing electric field is generated below it. The high-intensity electric field will cause edge and point corona discharge [14]. Appendix G of the GJB 8848-2016 standard gives the vertical electric field intensity and change rate at a distance of 10 m from the discharge channel, and the field intensity is close to 3×10^6 V/m.

Fig.4 HV electrode (3 m in diameter)

According to the simulation results, it is very difficult to establish such an electric field environment in the laboratory without flashover of the tested system. Therefore, the field environment simulated by the test system is mainly considered to meet the change rate of the electric field, namely reaching 6.8×10^{11} V/(m·s^{-1}). The actual test platform is shown in Fig. 4.

In addition, the simulation software CST is used for simulation, and the influence of the structure of the high-voltage electrode on the electric field distribution below is analyzed. As the tip discharge will distort the electric field under the electrode, the local field strength will increase and affect the field uniformity, as shown in Fig. 5. Therefore, the sharp parts of the high-voltage electrode are appropriately modified in the later stage.

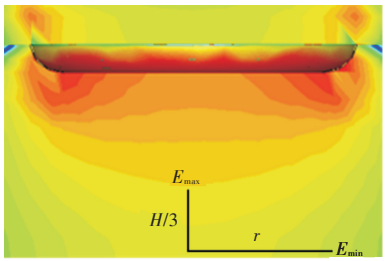

Fig. 5 Electric field distribution under the high voltage electrode

This paper proposed to verify whether the electric field meets the uniformity index by using the quantitative equation for uniformity, as shown in Eq. (1). When the electric field uniformity coefficient β is less than 3 dB, it is considered that the electric field uniformity under the high-voltage electrode is good. At the same time, the influence of the height H of the high-voltage electrode and the side length of the conductive ground plane on the field uniformity is analyzed. The simulation results show that for a high-voltage electrode with a diameter of 3 m when the height H is 2 m and the side length of the conductive ground plane is 3.5 m, the uniformity of the electric field below is good.

$$\beta = 20\lg\frac{E_{max}}{E_{min}} \tag{1}$$

where E_{max} and E_{min} are the maximum and minimum values of the electric field strength at the height of $H/3$ from the ground, respectively.

2.4 Measurement and control systems

The measurement and control systems mainly implement two functions of control and measurement.

The control system is mainly responsible for state monitoring and action control. By monitoring the voltage and current signals of the charge and discharge circuit in real-time, the computer determines and executes the control actions. Its operation interface includes a display area of status information and control area. The display area of status information shows the current setting parameters, status monitoring and fault information in real-time. The control area integrates charge and discharge, trigger, fault reset, emergency stop, and other control actions.

The measurement system includes a capacitive voltage divider and an electric field sensor, which measure the discharge circuit voltage and the test space electric field, respectively. The capacitive volt-

age divider makes partial voltage measurement of the impulse high-voltage and outputs the signal to the oscilloscope, completing the collection and preprocessing at the back-end workstation. The electric field sensor consists of an electric field probe and a light transmission device. The electric field probe is a dipole antenna used to monitor the electric field signal below the high-voltage electrode. The light transmission device converts the monitored electric field signal into an optical signal and transmits it to the photoelectric converter in the shielded cabinet. Then, it is converted into an electrical signal and output to the oscilloscope for measurement, thereby greatly reducing the influence of electromagnetic interference on the signal acquisition.

The detailed function description of the control and measurement system is shown in Table 1.

Table 1 Function description of control and measurement system

Name	Content	System function
Control system	State monitoring	Current voltage, current sphere gap, charging time, polarity status, fault, and gate interlock
	Control action	Main power switching on, charging, triggering, grounding, emergency stop, and fault resetting
Measurement system	Voltage measurement	Capacitive voltage divider
	Electric field measurement	Electric field probe and light transmission device

3 Test results and analysis

3.1 Full waveform

The electric field environment simulator for nearby lightning strikes outputs 1.2/50 μs full-waveform when it does not chop the wave by the cut-off device. Fig. 6 shows the normalized waveforms measured by the capacitive voltage divider and the electric field sensor when the single-stage charging voltage of Marx generator is 30 kV. The figure shows that the rise time of the two waveforms agrees well with the half-peak width. This shows that the full waveform output by the electric field environment simulator for nearby lightning strikes is stable and reliable, and the electric field sensor meets the measurement requirements of the electric field signal.

3.2 Chopped waveform

Fig. 7 shows the normalized chopped waveforms measured by the capacitive voltage divider and electric field sensor when the single-stage charging voltage of Marx generator is 30 kV. The figure shows that the rise time of the two is consistent with the half-peak width, and the drop time of the waveform is similar.

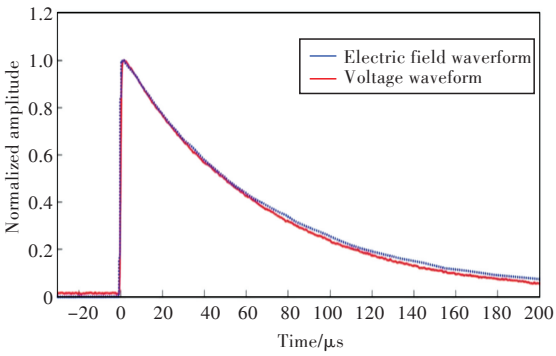

Fig.6 Normalization comparison of full waveform

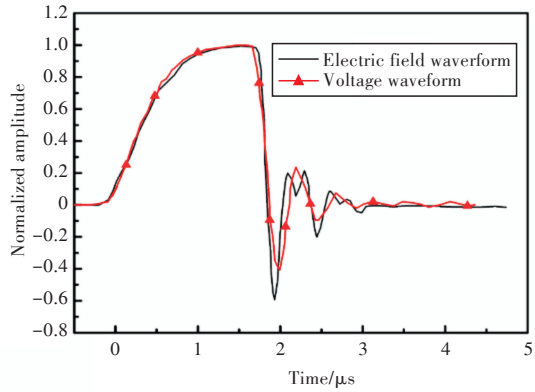

Fig.7 Normalization comparison of chop waveform

The maximum change rate of the electric field under the electrode can be approximately estimated by Eq. (2). According to the mean value theorem, the maximum value of the actual change rate is always greater than the estimated value.

$$\frac{\mathrm{d}E}{\mathrm{d}t}=\frac{U_{\max}}{1.67\,T_{\mathrm{d}}\,H} \tag{2}$$

where $\mathrm{d}E/\mathrm{d}t$ is the change rate of the electric field; $U_{\max}$ is the peak discharge voltage measured by the capacitive voltage divider, and H is equal to 2 m; T_{d} is the drop time (70%-10%).

Table 2 shows the cut-off time and drop time of the chopped waveform and the maximum change rate of the electric field calculated according to Eq. (2) when the single-stage charging voltage of the Marx generator is 15, 20, 25, 30, 35, and 40 kV, respectively. It is observed that

1) The cut-off time of the test device designed in this paper is shorter than 2 μs, which is basically cut off near the peak time and has a positive correlation with the charging voltage.

2) The drop time of the chopped wave is between 0.07 and 0.09 μs, which is basically independent of

Table 2 Time variation rate of electric field at different charging voltages

Single-satge charging voltage/kV	Volatge peak U_{max} /kV	Cut-off time T_c/μs	Drop time T_d/μs	Maximum dE/dt /(V·m^{-1}·s^{-1})
15	118.5	1.38	0.076 8	4.63×10^{11}
20	156.61	1.40	0.077 4	6.07×10^{11}
25	196.38	1.69	0.077 4	7.61×10^{11}
30	237.34	1.86	0.078 6	9.06×10^{11}
35	278.94	1.82	0.082 2	10.2×10^{11}
40	311.7	1.85	0.080 4	11.6×10^{11}

the charging voltage of the Marx generator.

3) Under the single-stage charging voltage of 25-40 kV, the maximum value of the electric field change rate is greater than 6.8×10^{11} V/(m·s^{-1}), which meets the requirements of GJB 1389A-2005. Moreover, with the increase in the charging voltage, the maximum change rate of the electric field increases.

When the height of the high-voltage electrode changes, the charging voltage of the Marx generator can be adjusted to make the change rate of the electric field in a certain space below the electrode meet the requirements. Therefore, the height of the high-voltage electrode from the device under test can be adjusted appropriately according to the discharge voltage level.

4 Conclusions

According to GJB 1389A-2005, a kind of electric field environment simulator for nearby lightning strikes is designed and developed in this paper. The test and application results show that

1) The simulation device can generate a standard 1.2/50 μs lightning full-wave, and the electric field and voltage waveforms basically match.

2) The simulation device can generate a chopped waveform, and it is not affected by the pre-discharge process of the gap to produce front-end distortion. The cut-off time is shorter than 2 μs, and the drop time is shorter than 0.09 μs.

3) When the single-stage charging voltage is from 25 kV to 40 kV, an electric field environment with a maximum change rate of electric field greater than 6.8×10^{11} V/(m·s^{-1}) can be generated in a certain space below the high-voltage electrode.

In summary, this device can generate an electric field environment of nearby lightning strikes that meets the requirements of GJB 1389A-2005 and can provide equipment support for the research on the indirect effect of the nearby lightning strikes on system electronic and electrical equipment.

References

[1] Pei G F, Chen H L, Gao C. Lightning protection evaluation technology of surface ship based on leader progression model [J]. High Power Laser and Particle Beams, 2018, 30(1): 013202 (in Chinese).

[2] Zheng S Q, Hou D Y, Feng D, et al. Lightning menace to ship and corresponding protection design requirements [C]//Proceedings of the 3rd Asia-Pacific Conference on Antennas and Propagation. Harbin, China: IEEE, 2014.

[3] Huang R T, Duan Y T, Shi L H, et al. Simulation analysis on return conductor configuration for lightning indirect effect test of metal cylinder[J]. Chinese Journal of Ship Research, 2018, 13(Supp 1): 66-70, 91 (in Chinese).

[4] Thomson E M. A critical assessment of the US code for lightning protection of boats[J]. IEEE Transactions on Electromagnetic Compatibility, 1991, 33(2): 132-138.

[5] Zhang Y J, Zhou X J. Review and progress of lightning research [J]. Journal of Applied Meteorological Science, 2006, 17(6): 829-834 (in Chinese).

[6] Zeng R, Zhou X, Wang Z Z, et al. Review of research advances and fronts on international lightning and protection[J]. High Voltage Engineering, 2015, 41(1): 1-13 (in Chinese).

[7] Commission of State Administration of Science, Technology and Industry for National Defence. Electromagnetic compatibility requirements for systems: GJB 1389A-2005 [S]. Beijing: PLA General Armament Department, 2005.

[8] State Administration of Science. Technology and Industry for National Defence. Electromagnetic environmental effects test methods for systems: GJB 8848-2016 [S]. Beijing: Armament Department of Central Military Commission, 2016.

[9] NPFC. Electromagnetic environmental effects requirements for systems: MIL-STD-464 [S]. [S.n.]: NPFC, 2010.

[10] NATO. Electromagnetic environmental effects test and verification: AECTP-500-4[S]. [S.n.]: NATO Standardization Agency, 2011.

[11] Zhao Z D. High voltage technique[M]. 3rd ed. Beijing: China Electric Power Press, 2013 (in Chinese).

[12] Xuan Y W, Le Y J, Zhang N F, et al. Method to determine wave resistance of impulse voltage generator for lightning impulse test[J]. Journal of Mechanical and Electrical Engineering, 2014, 31(3): 388-392 (in Chinese).

[13] Yang D W, Wang Y T, Shan Y S. Experimental research on the Marx-generator building time and jitter [J]. High Power Laser and Particle Beams, 2002, 14 (5): 775-777 (in Chinese).

[14] Shao T, Yan P. Atmospheric gas discharge and its plasma application [M]. Beijing: Science Press, 2015 (in Chinese).

邻近雷击电场环境模拟装置的设计与实现

王可, 段艳涛*, 石立华, 黄瑞涛, 陈海林
陆军工程大学 电磁环境效应与光电工程重点实验室,江苏 南京 210007

摘　要: [**目的**] 雷电对空阔海域上的舰船危害极大,特别是随着电子、电气设备及封闭式集成桅杆的大量应用,舰船雷电间接效应日趋严重。为了有效开展舰载电子、电气设备的雷电间接效应试验,[**方法**] 基于Marx发生器原理,设计并实现一种邻近雷击电场环境模拟装置。该装置利用可调单球隙实现冲击高压的峰值截断,通过高压极板与导电地平面建立邻近雷击电场模拟环境。[**结果**] 试验结果表明,该装置截断时间小于2 μs,跌落时间小于0.09 μs,能够产生符合GJB 1389A-2005要求的脉冲电场环境。[**结论**] 模拟装置可为依据GJB 8848-2016开展系统电子、电气设备的邻近雷击间接效应研究提供设备支持。

关键词: Marx发生器; 邻近雷击; 脉冲电场; 雷电间接效应

[*Continued from page* 53]

[17] Utiskul Y, Quintiere J G. Generalizations on compartment fires from small-scale experiments for low ventilation conditions[J]. Fire Safety Science, 2005, 8:1229-1240.
[18] Utiskul Y. Theoretical and experimental study on fully-developed compartment fires[D]. College Park, MD: University of Maryland, 2006.
[19] Li Q. Experimental study on smoke properties in a ship room with ceiling vent[D]. Hefei: University of Science and Technology of China, 2013 (in Chinese).
[20] Li T C. Simulation study on fire temperature and flue gas law in enclosed cabin of ships[D]. Guangzhou: South China University of Technology, 2017 (in Chinese).
[21] Li J, Pu J Y, Yu L F. Study on the general rule of fire in a ship cabin[J]. Technology Wind, 2017 (18): 236-237 (in Chinese).
[22] Chen B, Lu S X, Li C H, et al. Unsteady burning of thin-layer pool fires[J]. Journal of Fire Sciences, 2012, 30(1): 3-15.
[23] Chen B, Lu S X, Li C H, et al. Initial fuel temperature effects on burning rate of pool fire[J]. Journal of Hazardous Materials, 2011, 188(1/2/3): 369-374.

水平开口有限空间油池火燃烧特性分析

陈兵*[1], 张世奇[1], 时训先[1], 黎昌海[2], 陆守香[2]
1 中国安全生产科学研究院,北京 100012
2 中国科学技术大学 火灾科学国家重点实验室,安徽 合肥 230027

摘　要: [**目的**] 船舶机舱等有限空间通常具有顶部水平开口,开口位置和形状的特殊性导致其火灾燃烧特性与建筑火灾有着明显的区别。为了解和认识船舶机舱等顶部水平开口的火灾特性,[**方法**] 通过改变开口面积和庚烷油池的尺寸,开展顶部开口有限空间火焰熄灭模式、火焰形态与燃烧速率等燃烧特性的实验研究。[**结果**] 根据火灾熄灭原因,有限空间火灾发展过程分为O_2浓度不足导致的"缺氧熄灭"模式和可燃物耗尽导致的"燃料耗尽熄灭"模式。在"缺氧熄灭"模式中,烟气混合物被卷吸进入火焰参与燃烧过程,火焰自熄灭临界O_2浓度处于13%~16.5%,且火焰形态由稳定燃烧的形状变成在脱离油池并不断游走的状态。在"燃料耗尽熄灭"模式下,火焰形态较为稳定,并且由于沸腾燃烧导致燃烧后期燃烧速率有较为明显的增大。[**结论**] 研究结果展示了顶部开口有限空间火灾的燃烧特性,对了解船舶舱室火灾的发展过程具有重要意义,并为船舱火灾扑救提供了理论支持。

关键词: 顶部水平开口; 有限空间; 油池火; 燃烧特性